Chemical Science

ROYAL SOCIETY OF CHEMISTRY

EDGE ARTICLE

View Article Online
View Journal | View Issue

Cite this: *Chem. Sci.*, 2026, **17**, 205

All publication charges for this article have been paid for by the Royal Society of Chemistry

Graphene oxide/carbon nanotube reinforced PCM microcapsules with high thermal conductivity and high latent heat for thermal energy storage

Bowei Du,[ab] Xinbing Jiang,[ab] Zhijie Zhang,[ab] Kai Xi,[ab] Borui Zhang,[c] Qinghao Yang[c] and Shujiang Ding *[ab]

Received 8th September 2025
Accepted 15th October 2025

DOI: 10.1039/d5sc06909b

rsc.li/chemical-science

Efficient thermal energy storage requires phase change materials (PCMs) with both high latent heat and enhanced thermal conductivity. Here, polymethyl methacrylate (PMMA)-based PCM microcapsules were synthesized *via* emulsion polymerization with interfacial self-assembly, incorporating graphene oxide (GO) and carbon nanotubes (CNTs) as conductive fillers. Optimization of emulsifier type and shell-to-core ratio improved morphology and encapsulation, with a 0.50 ratio achieving 67.7% high loading and latent heat exceeding 165 J g^{-1}. Comprehensive characterization (FTIR, Raman, XRD, XPS) confirmed strong interfacial interactions between fillers and polymer shells. The combined addition of GO and CNTs reduced leakage, increased latent heat retention by over 12%, and yielded uniform capsule morphology. Infrared thermal imaging further revealed that PCM-GO/CNTs microcapsules exhibited slower cooling, more stable temperature plateaus, and superior heat storage performance compared with control and single-filler systems. These findings highlight the effectiveness of hybrid GO/CNT incorporation in enhancing both structural stability and thermal regulation, offering a promising route for advanced thermal energy storage applications.

Introduction

Electrochemical energy storage has emerged as a leading technology due to its high specific energy, superior efficiency, environmental compatibility, and independence from geographical limitations.[1,2] However, large-scale deployment inevitably generates substantial heat, and performance degradation under extreme conditions, coupled with safety concerns such as thermal runaway, remain pressing challenges.[3,4] Effective temperature regulation is therefore critical to suppress capacity fading, extend service life, and enhance operational safety.[5–7] Compared with conventional cooling strategies, phase change cooling offers distinct advantages by maintaining cell temperatures within an optimal range and minimizing inter-cell gradients without extra energy input.[8–12] Yet, the intrinsic drawbacks of pure organic or inorganic phase change materials severely restrict their scalability.[13–15] Phase change composites provide a promising solution by integrating the merits of both classes, achieving high latent heat, enhanced thermal stability, and improved thermal conductivity.[16–20] These attributes position them as strong candidates for next-generation passive cooling systems, highlighting the urgent need to design high-performance PCM composites for practical energy storage applications.

Encapsulating PCMs effectively mitigates leakage, while imparting high heat storage efficiency, large surface area, and resistance to corrosion and overcooling.[21–25] Incorporating thermally conductive fillers and surface functionalization strategies have further improved the thermal conductivity of PCM microcapsules,[26–30] yet these advances remain insufficient to meet the stringent demands of high-rate cycling in electrochemical systems.[31,32] In polymer-based composites, interfacial thermal resistance between fillers and the polymer maxtrix-as well as between adjacent fillers—largely determines overall conductivity.[33–36] Conventional strategies that randomly disperse fillers within the matrix often cause agglomeration, requiring high filler loadings to form continuous pathways.[37–39] This not only increases cost and complicates processing but also compromises mechanical integrity. Constructing interconnected thermal networks therefore represents a more effective strategy, as it promotes phonon transport, reduces interfacial resistance, and enhances overall thermal conductivity.[40] Such an approach holds great promise for enabling high-performance PCM composites tailored for advanced thermal management applications.

[a]*School of Chemistry, Engineering Research Center of Energy Storage Materials and Devices, Ministry of Education, National Innovation Platform (Center) for Industry-Education Integration of Energy Storage Technology, Xi'an Jiaotong University, Xi'an 710049, China. E-mail: dingsj@mail.xjtu.edu.cn*

[b]*State Key Laboratory for Electrical Insulation and Power Equipment, Xi'an Jiaotong University, Xi'an 710049, China*

[c]*School of Materials Science and Engineering, Xi'an University of Science and Technology, Xi'an 710054, China*

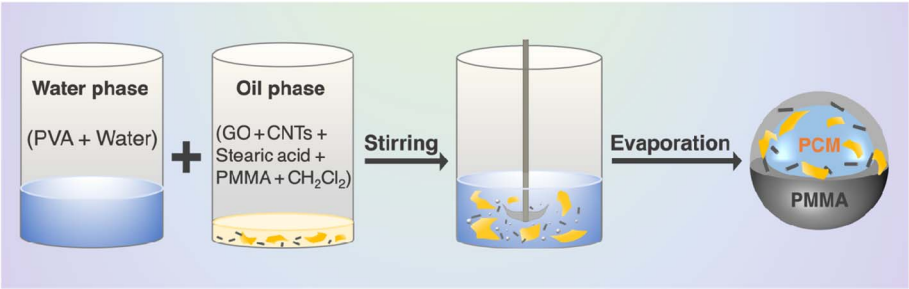

Scheme 1 Schematic illustration of the synthesis of the PCM-GO/CNTs microcapsules.

In this work, we developed low-cost, high-efficiency phase-change microcapsules (PCM-GO/CNTs) using PMMA as the shell, stearic acid (melting point ~70 °C) as the phase-change core, and PMMA-modified graphene oxide and carbon nanotubes as thermally conductive fillers (Scheme 1). The capsules were synthesized *via* a simple emulsion-evaporation method, in which GO and CNTs anchored within the shell framework are expected to form efficient conductive pathways, thereby reducing interfacial resistance and enabling effective phonon transport at low filler loadings. The effects of emulsifier type and content, as well as shell–core ratio, were systematically investigated with respect to microstructure, thermal stability, leakage resistance, and heat storage behavior. This fatty acid-based PCM system demonstrates strong potential for thermal energy storage and provides a versatile design strategy for advanced multifunctional composites.

Results and discussion

Emulsifiers play a crucial role in stabilizing emulsions. To identify the optimal emulsifier, PCM microcapsules were synthesized using polyvinyl alcohol (PVA) emulsifiers of different molecular weights (PVA-0588, PVA-1788, and PVA), and their morphologies were examined using optical microscopy (OM). As shown in Fig. 1a, microcapsules prepared with PVA-0588 exhibited low encapsulation efficiency, with a large amount of PMMA aggregation resulting from failed synthesis. These microcapsules also displayed irregular morphologies and poor particle size distribution. In contrast, the use of PVA-1788 markedly improved synthesis efficiency and capsule uniformity. Nevertheless, the OM image still revealed a considerable number of defective microcapsules, characterized by aggregated polymer clumps that compromised encapsulation efficiency. A further improvement was achieved with PVA of molecular weight 67 000, which produced microcapsules with high encapsulation efficiency and uniform particle size distribution, with little evidence of PMMA aggregation compared to the other two emulsifiers. These findings indicate that emulsifier molecular weight has a significantly effect on microcapsule formation and encapsulation efficiency: lower molecular weights lead to poor encapsulation efficiency, whereas increasing molecular weight within a certain range enhances performance. To further investigate the effect of emulsifier content, PCM microcapsules were synthesized using PVA-67000 at three different dosages (0.3, 0.5, and 1 g). As shown in Fig. 1b, increasing emulsifier content substantially reduced microcapsule yield, with 0.3 g providing the best synthesis efficiency and particle size distribution. Scanning electron microscopy (SEM) observations of microcapsules with different emulsifier contents confirmed the OM results, demonstrating that synthesis efficiency decreases with increasing emulsifier concentration (Fig. 1c). Furthermore, in the absence of graphene oxide (GO) as a stabilizer, the microcapsules exhibited a pronounced leakage rate, as clearly visible in the electron microscopy images. Even at the optimal emulsifier content of 0.3 g, the encapsulation success rate remained relatively low.

Thermally conductivity is optimized when the thermally conductive materials is uniformly dispersed throughout the PCM microcapsule structure. Therefore, it is crucial to ensure uniform dispersion of graphene oxide (GO) in the oil phase (PMMA disssolved in dichloromethane). As demonstrated in our experiments, pre-silanization of GO effectively improves its dispersibility and stability in the oil phase (Fig. S1). We synthesized PCM microcapsules with different thermally conductive material combinations and treatments, including GO alone, untreated GO/CNTs, and PMMA-modified GO/CNTs (with 0.5 wt% GO and 1 mg CNTs, respectively). OM and SEM images of the microcapsules' morphology and microstructure revealed significant improvements in encapsulation efficiency and surface uniformity with the addition of 0.5 wt% GO, compared to untreated PCM microcapsules. This demonstrates that the addition of GO effectively enhances PCM encapsulation stability (Fig. 2a and d). However, encapsulation efficiency remained low, especially after incorporating the one-dimensional conductive material, CNTs, which led to cracks on the surface of the synthesized microcapsules. These cracks could cause leakage during the phase change process of the PCM. The cause of this issue lies in the uneven distribution of the thermally conductive material in the oil phase, which becomes more pronounced as the solvent evaporates during microcapsule formation (Fig. 2b and e). This problem is effectively addressed by adding silanized thermally conductive materials. Fig. 2c and f show that PCM microcapsules prepared with PMMA-modified GO and CNTs exhibit a uniform particle size distribution and smooth surface morphology.

The SEM and TEM images in Fig. 3a–c demonstrate that all microcapsules exhibit a regular spherical morphology with a stable core–shell structure, which is crucial for their thermal

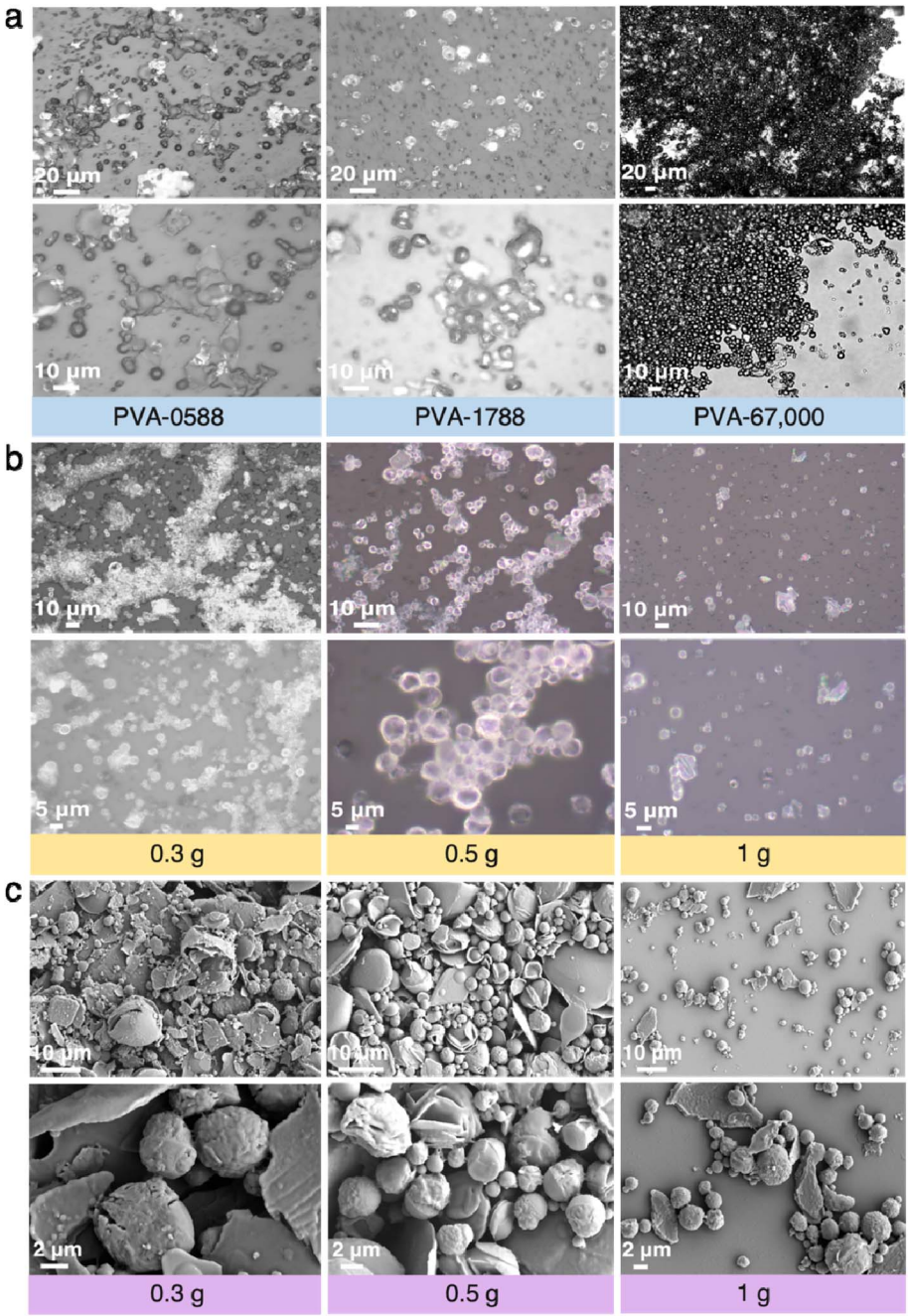

Fig. 1 Optical images of PCMs microcapsules with different (a) emulsifier types, and (b) content of PVA-67,000. (c) SEM images of PCM microcapsules with different content of PVA-67,000.

and mechanical stability. The size distribution of the PCM-GO/CNTs microcapsules ranges from 1.2 to 4.6 μm. Furthermore, Fig. 3b and c clearly reveal that the outer shell of the PCM-GO/CNTs microcapsules is coated with GO, indicating that GO is firmly attached to the shell surface. The wavy, cloud-like morphology of the GO sheets, without noticeable agglomeration, ensures a more effective dispersion of the thermally conductive filler, which enhances the overall heat transfer capability of the microcapsules. Fourier transform infrared (FTIR) spectroscopy was employed to analyze the interactions among PCMs, the polymer, and thermally conductive fillers. As shown in Fig. 3d, the FTIR spectra of PMMA, stearic acid (SA), PCM microcapsules, PCM-GO microcapsules, and PCM-GO-CNTs microcapsules exhibit characteristic absorption peaks. In the spectrum of pure PMMA, the strongest peak at 1731 cm^{-1} corresponds to the carbonyl (C=O) group, while the strong peak at 1143 cm^{-1} is attributed to C–O–C stretching vibrations.[41] For pure SA, the peak at 1702 cm^{-1} arises from C=O stretching vibrations.[42] In addition, the peaks at 2848 cm^{-1} and 2916 cm^{-1} correspond to the symmetric and asymmetric

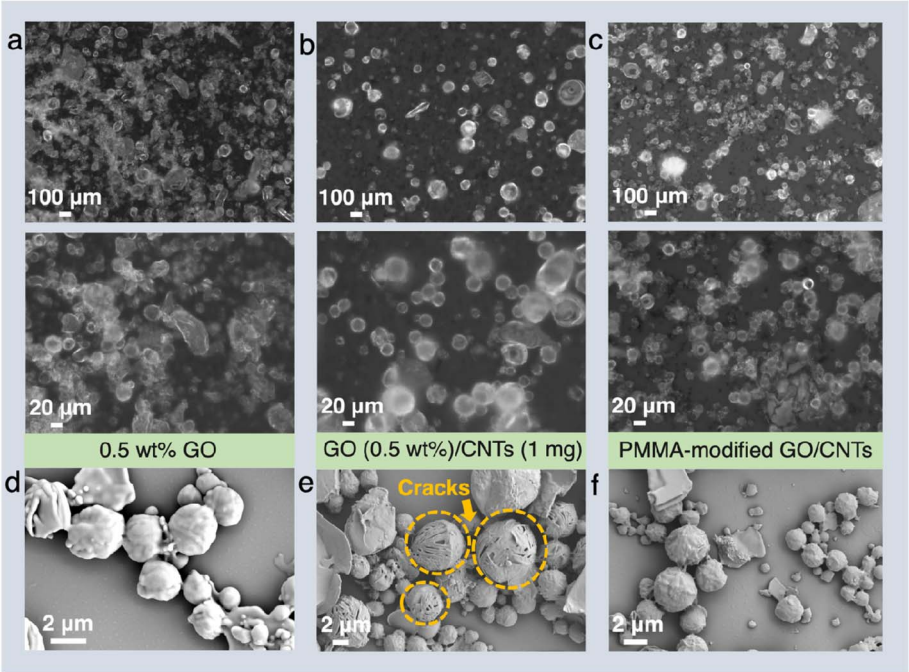

Fig. 2 Optical and SEM images of PCMs microcapsules with different high-conductivity materials (a) and (d) 0.5 wt% GO, (b) and (e) GO (0.5 wt%)/CNTs (1 mg) without any modification, (c) and (f) with PMMA-modified GO (0.5 wt%)/CNTs (1 mg).

stretching vibrations of the C–H bond in the $-CH_2$ group, respectively. Because only small amounts of GO and CNTs were added, no new characteristic peaks were observed in the spectra of the composite microcapsules. This suggests that the encapsulation process between PMMA and SA involves physical bonding rather than chemical reactions, thereby ensuring ensures the stability of the PCMs. Raman spectroscopy further confirmed the successful incorporation of GO and CNTs. As shown in Fig. 3e, the spectra of PCM-GO and PCM-GO/CNTs microcapsules display the characteristic D and G bands of GO at 1361 cm^{-1} and 1592 cm^{-1}, respectively. This confirms that GO is well integrated into the microcapsule shell, improving the thermal conductivity and mechanical strength of the microcapsules. The characteristic CNT peak at 2700 cm^{-1} was not observed, likely due to the low CNTs loading (1 mg) in the PCM-GO/CNTs microcapsules. All three types of microcapsules exhibited two strong peaks at 2848 cm^{-1} and 2957 cm^{-1}, with the latter corresponding to C–H stretching vibrations, while the former is associated with $O–CH_3$ vibrations.[43] These Raman features are consistent with the reported spectra of PMMA, further confirmed the successful encapsulation and structural stability of the PCM microcapsules, while the incorporation of GO and CNTs enhances heat transfer efficiency, mechanical properties, and thermal energy storage performance.

X-ray photoelectron spectroscopy (XPS) was conducted to further investigate the interactions between GO and PCM microcapsules, confirming the strong bonding among GO, CNTs, and PCM microcapsules. As shown in Fig. 3f, the full XPS spectra of PCM microcapsules and PCM-GO/CNTs microcapsules both display two distinct peaks corresponding to O 1s and C 1s. The calculated C/O atomic ratio of the PCM-GO/CNTs microcapsules (3.26) is notably higher than that of the PCM microcapsules (2.97), indicating successful incorporated of GO/CNTs and their exposure on the microcapsule surface, which increases the overall carbon content. This provides further evidence of strong interfacial bonding between the thermally conductive fillers and the PCM microcapsules. The high-resolution C 1s spectra of both PCM and PCM-GO/CNTs microcapsules exhibit three characteristic peaks (Fig. 3g). Peaks at 283.63 and 287.88 eV are assigned to C–C/C–H (aliphatic) bonds and C═O/O–C═O bonds, respectively. The introduction of GO and CNTs induces π–π interactions with PCM and stearic acid, as well as hydrogen bonding and dipole interactions between carbonyl groups and oxygen-containing functional groups (*e.g.*, –OH) on GO. These interactions facilitate electron transfer from the polymer matrix to the nanofillers, reducing the electron cloud density of carbon atoms. As a result, the binding energy of carbon atoms increases, leading to a leftward shift of the two characteristic C 1s peaks. Furthermore, the increase in overall carbon content and the reduced relative area of carbonyl-related peaks are consistent with the higher C/O ratio observed in the survey spectra.

The crystal structures of PCM microcapsules, PCM-GO microcapsules, PCM-GO/CNTs microcapsules, PMMA, and pure SA were analyzed by X-ray diffraction (XRD) as shown in Fig. 3h and S3.[41] All three PCM microcapsule samples exhibit distinct diffraction peaks at 11.20°, 21.64° and 24.19°, corresponding to the (005), (110) and (021) crystal planes of SA. These strong and sharp diffraction peaks confirm the presence of crystalline SA within the microcapsules. However, consistent with previous studies, the characteristic diffraction peaks of GO and CNTs are not observed in the wide-angle XRD patterns,

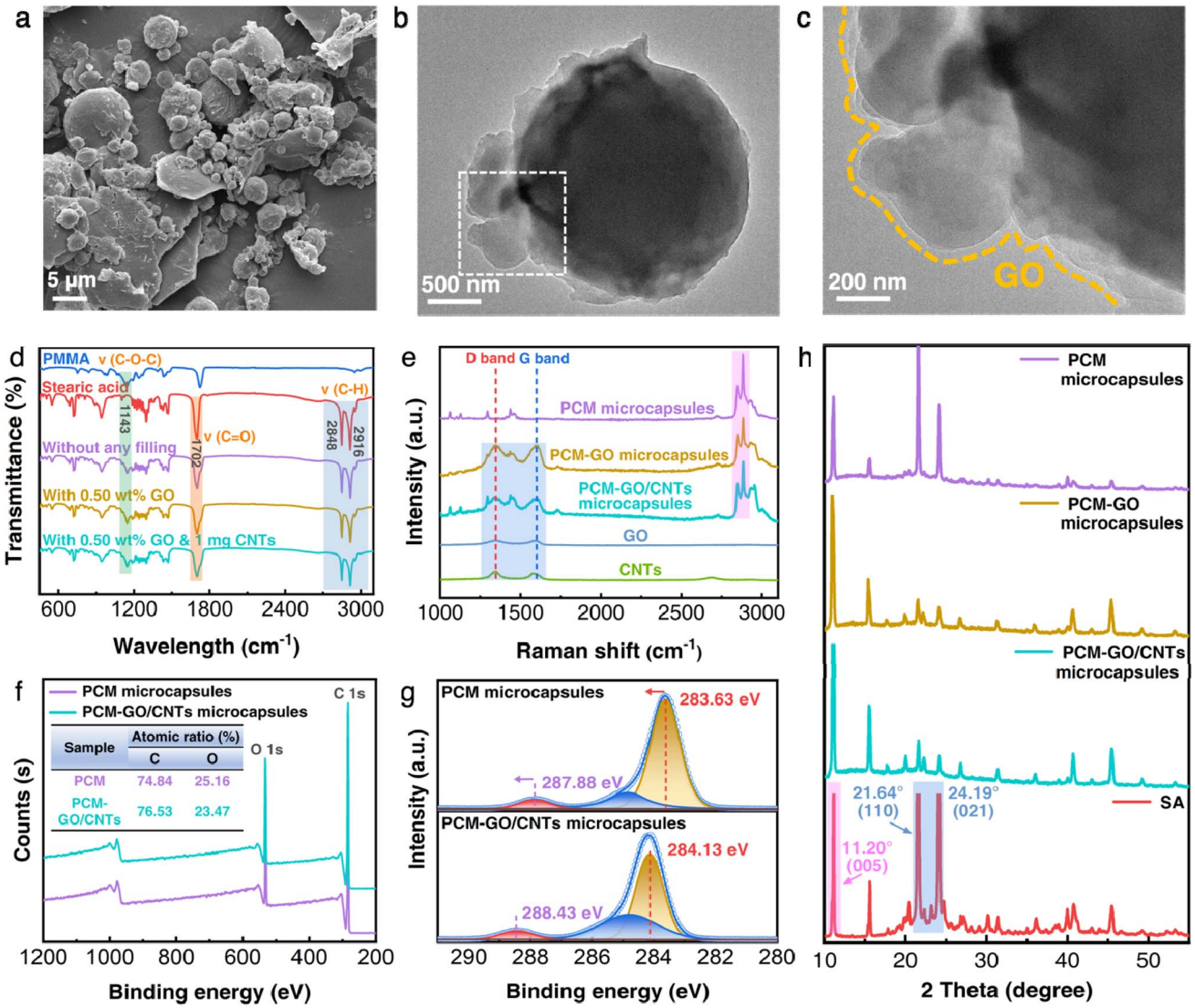

Fig. 3 (a) SEM, (b) and (c) TEM images of PCM-GO/CNTs microcapsules. (d) FTIR spectra of (1) pure PMMA, (2) pure stearic acid, (3) 0.50 shell/core ratio of PCMs microcapsules, (4) 0.50 shell/core ratio with 0.5 wt% GO, and (5) 1.0 mg CNTs of PCMs-GO (0.5 wt%) microcapsules. (e) Raman scattering spectra of the PCM microcapsules, PCMs-GO microcapsules, PCMs-GO/CNTs microcapsules, GO and CNTs. (f) XPS spectra and (g) high-resolution C 1s spectra of PCM microcapsules and PCM-GO/CNTs microcapsules. (h) XRD patterns of (1) 0.50 shell/core ratio of PCMs microcapsules, (2) 0.50 shell/core ratio with 0.5 wt% GO, (3) 1.0 mg CNTs of PCMs-GO (0.5 wt%) microcapsules and (4) pure stearic acid.

likely due to their low loading in the composite microcapsules. The successful incorporation of GO and CNTs is instead verified by Raman spectroscopy and TEM observations.

The shell-to-core mass ratio is a critical parameter that determines the amount of coating material in PCM microcapsules, thereby directly influencing encapsulation efficiency and energy storage capacity. As shown in Fig. S2, PCMs microcapsules were prepared with different shell–core ratios and their compositions and phase transition behaviors were evaluated by thermogravimetric analysis (TGA) and differential scanning calorimetry (DSC). The shell-to-core mass ratio was varied from 0.25 to 0.50 and 0.75, and the actual values were obtained from TGA data (Table 1). TGA results reveal that pure SA begins to evaporate at 200 °C and completes mass loss at 330 °C in a single step, indicating simple evaporation (Fig. 4a). In contrast, PCM microcapsules exhibit two distinct weight-loss stages between 150–430 °C: the first corresponds to the evaporation of encapsulated SA, while the second arises from the decomposition temperature of the PMMA shell, ending near 430 °C.[44] The increased initial decomposition temperature of SA

Table 1 Content of PCMs microcapsules with different shell and core ratios

Shell : Core	Content of shell (%)	Content of core (%)	Ratio of shell & core (%)
0.25	27.73	72.27	38.37
0.50	32.27	67.73	47.65
0.75	39.77	60.23	66.03

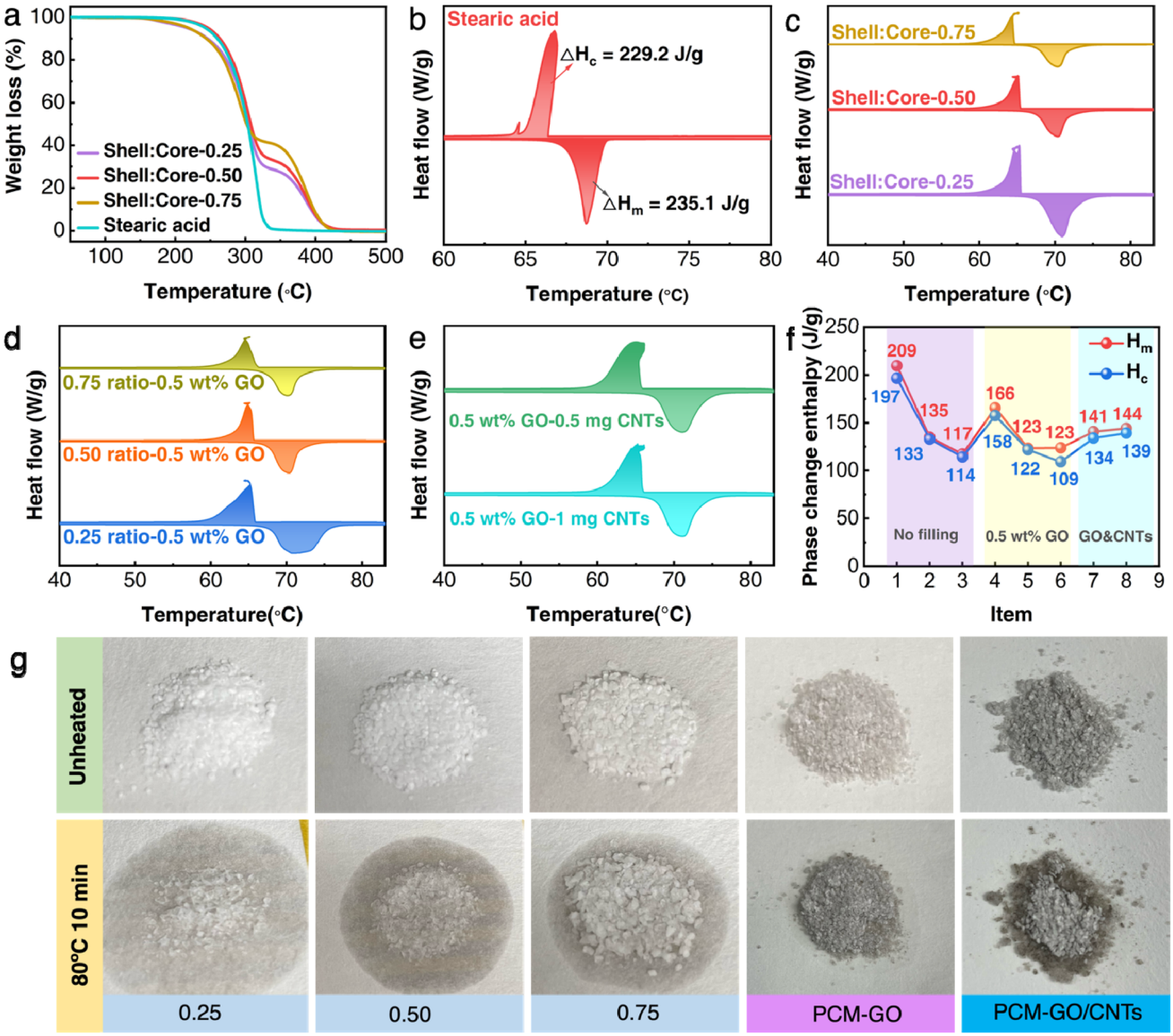

Fig. 4 (a) TGA, and DSC curves comparing (b) pure stearic acid with (c) PCMs microcapsules of different shell/core ratios. (d) Different shell/core ratio with 0.5 wt% GO, and (e) 0.5 mg and 1.0 mg CNTs of PCMs-GO (0.5 wt%) microcapsules. (f) Phase change enthalpies of PCMs microcapsules with different high-conductivity materials, including (1) different shell/core ratio (0.25, 0.50, and 0.75) without filling; (2) different shell/core ratio (0.25, 0.50, and 0.75) with 0.5 wt% GO; (3) same shell/core ratio (0.50) and 0.5 wt% GO filling with 0.5 mg and 1.0 mg CNTs. (g) Leakage tests of diferent ratio (0.25, 0.50, 0.75) of PCM microcapsule, PCM-GO microcapsules and PCM-GO/CNTs microcapsules.

within the microcapsules indicates that encapsulation improves its thermal stability, and a thicker shell provides greater protection. Among the tested ratios, a shell-to-core ratio of 0.50 closely matched the actual ratio of the prepared microcapsules and yielded a PCM loading of 67.73%. Although this is only 25% lower than that of the 0.25 ratio, the encapsulation ratio is reduced by less than 5% (4.54%). Therefore, a 0.50 ratio is considered the optimal formulation for PCM microcapsules.

The thermal storage behavior was further investigated by DSC (Fig. 4b). Pure SA exhibits a sharp endothermic peak at 68.7 °C with a melting enthalpy of 235.1 J g^{-1}, and an exothermic peak at 66.8 °C with a crystallization enthalpy of 229.2 J g^{-1}. For the PCM microcapsules, the latent heat of phase change increases as the core-to-shell ratio decreases from 0.75 to 0.50 to 0.25, owing to the higher proportion of encapsulated SA, consistent with TGA results (Fig. 4c). The incorporation of 0.5 wt% GO into microcapsules with different core-to-shell ratios caused both melting and crystallization temperatures to decrease relative to samples without GO, reflecting restricted crystallization of SA within the microcapsules. The melting enthalpies of these microcapsules were 123.7, 123.3, and 165.5 J g^{-1}, values comparable to those of microcapsules without thermal conductive fillers (Table 2 and Fig. 4d). Notably, the difference in melting enthalpy between the 0.25 and 0.50 ratios decreased from 35.6% (without GO) to 25.5% (with GO), representing a 10.1% reduction in enthalpy loss. This

Table 2 DSC analysis of PCMs microcapsules under various synthesis conditions

Sample	Shell:core	Thermal conductivity filling	Melting		Solidifying	
			T_m (°C)	ΔH_m (J g^{-1})	T_c (°C)	ΔH_c (J g^{-1})
1	0.75	—	70.3	117.3	65.0	114.1
2	0.50	—	70.5	134.9	65.0	132.8
3	0.25	—	71.0	209.4	65.4	196.5
4	0.75	0.5 wt% GO	70.2	123.7	64.6	109.1
5	0.50	0.5 wt% GO	70.4	123.3	64.9	121.7
6	0.25	0.5 wt% GO	70.6	165.5	65.2	157.5
7	0.50	0.5 wt% GO & 0.5 mg CNTs	71.1	140.6	65.1	133.9
8	0.50	0.5 wt% GO & 1.0 mg CNTs	71.2	144.1	65.3	139.1
Stearic acid	—	—	68.7	235.1	66.8	229.2

improvement is attributed to the emulsifying effect of GO, which enhances encapsulation efficiency and reduces PCM leakage.

Interestingly, the addition of CNTs further enhanced energy storage capacity. As a core–shell ratio of 0.50 with 0.5 wt% GO, the inclusion of CNTs increased the enthalpy by 12.3% (0.5 mg CNTs) and 14.8% (1.0 mg CNTs), compared with microcapsules without CNTs (Fig. 4e). The resulting PCM-GO/CNTs microcapsules achieved a phase-change enthalpy retention of ~61.3%, with a latent heat exceeding 144 J g^{-1}, which is suitable for thermal energy storage applications. As summarized in Fig. 4f, the addition of GO improves encapsulation efficiency and mitigates PCM loss across different shell-to-core ratios, while the synergistic combination of one-dimensional CNTs and two-dimensional GO further enhances latent heat capacity by more than 12%. This highlights the beneficial role of hybrid thermally conductive fillers in optimizing both the microcapsule preparation process and the energy storage performance of PCMs.

The leakage resistance of all microcapsule samples was evaluated by heating them at 80 °C for 10 min, a temperature above the phase transition point of SA (T_m = 69–72 °C) (Fig. 4g). As the shell-to-core ratio increased from 0.25 to 0.75, the leakage rate of microcapsule decreased, which can be attributed to the thicker shell providing higher encapsulation density, as well as the reduced PCM content at higher shell fractions leading to less potential leakage. To further examine the effect of thermally conductive fillers, leakage tests were conducted on microcapsules with a shell-to-core ratio of 0.50, containing either 0.5 wt% GO (PCM-GO) or a combination of 0.5 wt% GO and 1 mg CNTs (PCM-GO/CNTs). The incorporation of GO significantly reduced leakage compared with microcapsules without GO, with only a small amount of PCM observed at the capsule periphery, confirming that GO improves encapsulation efficiency. Remarkably, almost no detectable leakage occurred in PCM-GO/CNTs microcapsules. This suggests that CNTs may be distributed within the capsules shell in a manner that fills voids left by GO, thereby further enhancing the integrity of the barrier layer. Overall, PCM-GO/CNTs microcapsule exhibited the best anti-leakage performance among all tested samples.

To investigate the thermal storage performance of the phase-change microcapsules, an infrared thermal imager was employed to examine the heat absorption and release behaviors of PCM-GO and PCM-GO/CNTs microcapsules containing different thermally conductive fillers, along with a control group of PCM microcapsules without fillers. The samples were heated to 80 °C and then naturally cooled to 31 °C at room temperature. As shown in Fig. 5a and b, the PCM microcapsules containing thermally conductive fillers exhibited pronounced temperature hysteresis around 65 °C. In contrast, the temperature of the microcapsules without thermally conductive fillers rose and fell rapidly, indicating that the incorporation of thermally conductive fillers enhanced the heat storage capacity of the microcapsules. More importantly, the hysteresis plateau of

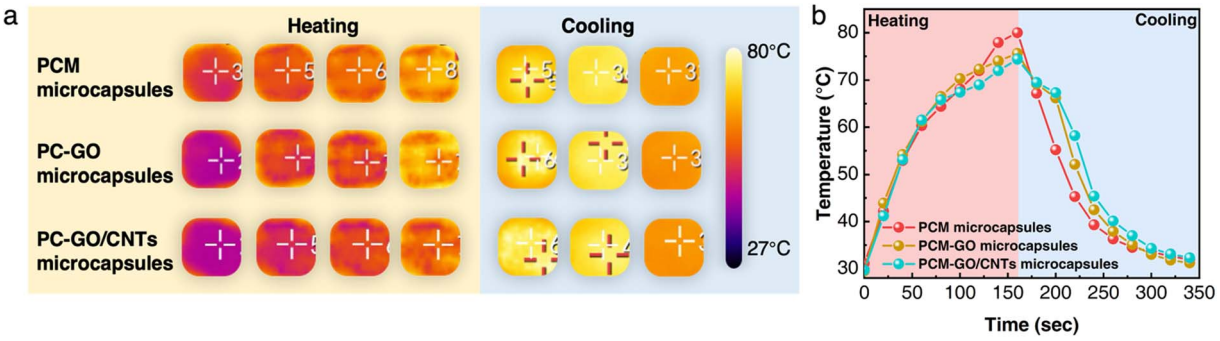

Fig. 5 (a) Infrared thermographic images and (b) plots of temperature evolution as a function of time for PCM microcapsule, PCM-GO microcapsules and PCM-GO/CNTs microcapsules.

the microcapsules containing CNTs was broader and flatter compared to that of the microcapsules without CNTs. During the cooling process, their temperature remained consistently higher than that of the control group at the same time point, demonstrating that PCM-GO/CNTs microcapsules possessed the best thermal storage performance among all samples. Overall, the infrared thermal analysis confirms that the synergistic incorporation of GO and CNTs not only improves the structural integrity of the microcapsules but also significantly enhances their thermal conductivity and latent heat retention. This dual effect underlines the potential of PCM-GO/CNTs microcapsules as efficient thermal energy storage materials for practical applications.

Conclusion

In this work, PCM microcapsules were synthesized through emulsion polymerization and interfacial self-assembly, achieving high encapsulation efficiency and enhanced thermal performance. The emulsifier molecular weight and shell-to-core ratio proved critical, with PVA (M_w = 67 000) and a ratio of 0.50 yielding 67.73% PCM loading and excellent thermal stability. Incorporation of GO enhanced filler dispersion, reduced leakage, and improved encapsulation efficiency, while the synergistic combination of GO and CNTs further reinforced the shell structure, minimized surface defects, and increased phase-change enthalpy by over 12% compared to GO-only systems. Structural analyses confirmed robust core–shell morphology and effective filler integration. Overall, the synergistic use of two-dimensional GO with one-dimensional CNTs provides a reliable approach to designing high-performance PCM microcapsules with superior energy storage efficiency and leakage resistance, enabling advanced applications in thermal management and energy storage.

Author contributions

Bowei Du: conceptualization, investigation, methodology, software, analysis, writing. Xinbin Jiang: resources. Zhijie Zhang: Raman tests. Kai Xi: resources. Borui Zhang: investigation. Qinghao Yang: resources. Shujiang Ding: supervision, funding acquisition. All authors contributed to the manuscript and approved the final version of the manuscript.

Conflicts of interest

There is no conflicts of interest to report.

Data availability

All data are given in the manuscript and the supplementary information (SI). The data supporting this article have been included as part of the SI. Supplementary information: additional experimental details and electrochemical tests, computational methods as well as SI figure (Fig. S1–S3). See DOI: **https://doi.org/10.1039/d5sc06909b**.

Acknowledgements

This work was supported by the National Natural Science Foundation of China (No. 52273081, 52433002, and 22278329), the Postdoctoral Research Project of Shaanxi Province (2023BSHYDZZ51), the Shaanxi Province Natural Science Foundation Youth Program (2025JC-YBQN-778), the Natural Science Basic Research Program of Shaanxi (No. 2022TD-27), and Key Projects of Shaanxi Province, China (2023GXLH-001). The authors deeply acknowledge the Instrument Analysis Center of Xi'an Jiaotong University for the SEM, TGA, DSC and OM tests, including Dr Jia Liu for the Raman spectroscopy, and Dr Chao Li for the TEM analysis. B. W. D. acknowledges his wife Mrs Pu Li, Dr Weilin Wang, Dr Zhongshuai Liang for their kindly advice. Authors appreciate eceshi (**www.eceshi.com**) for XPS, thermal conductivity tests.

References

1 K. Yan, Z. Lu, H. W. Lee, F. Xiong, P. C. Hsu, Y. Li, J. Zhao, S. Chu and Y. Cui, *Nat. Energy*, 2016, **1**, 1–8.
2 M. K. Aslam, Y. Niu, T. Hussain, H. Tabassum, W. Tang, M. Xu and R. Ahuja, *Nano Energy*, 2021, **86**, 106142.
3 B. B. Jing and C. M. Evans, *J. Am. Chem. Soc.*, 2019, **141**, 18932–18937.
4 T. Zhang, J. Yu, H. Guo, J. Qi, M. Che, M. Hou, P. Jiao, Z. Zhang, Z. Yan, L. Zhou, K. Zhang and J. Chen, *Chem. Soc. Rev.*, 2024, **53**, 12043–12097.
5 G. V. Kuznetsov and E. V. Kravchenko, *J. Energy Storage*, 2023, **65**, 107384.
6 K. Li, L. Wang, Y. Wang, X. Feng, F. Jiang and M. Ouyang, *eScience*, 2024, **4**, 100226.
7 K. Weng, M. Xu, M. Liu, X. Xu, P. Zheng, W. Qu, H. Huang, D. Liu, H. Jiang, Y. Zhang and D. Zou, *Renewable Energy*, 2025, **255**, 123803.
8 Z. Kang, X. Wang, R. Yin, L. Xu, J. Wu, S. Wang and Q. Peng, *Appl. Therm. Eng.*, 2025, **273**, 1–15.
9 Y. Sun, H. Zhang, F. Qi, Y. Li, H. Guo, C. Wang and Y. Chen, *Appl. Therm. Eng.*, 2025, **278**, 127194.
10 Q. Xu, H. Huang, Y. Gu, X. M. Lin, K. Zhu, M. Yin, L. Li, X. Wang and K. Zheng, *Appl. Therm. Eng.*, 2025, **266**, 125639.
11 Y. Gao, X. Chen, X. Jin, C. Zhang, X. Zhang, X. Liu, Y. Li, Y. Li, J. Lin, H. Gao and G. Wang, *eScience*, 2024, **4**, 100292.
12 N. Napa, M. K. Agrawal and B. Tamma, *J. Energy Storage*, 2023, **73**, 109119.
13 H. Lei, X. Wang, Y. Li, H. Xie and W. Yu, *Energy*, 2024, **304**, 132169.
14 J. Zhang, J. Mu, S. Chen and F. Xu, *J. Energy Chem.*, 2022, **75**, 229–239.
15 Q. Su, G. Sheng, Y. Li, X. Lu, C. Wang, C. Xin, H. Wang and H. Jiang, *J. Bionic Eng.*, 2025, **22**, 513–561.
16 Y. Zhang, P. Wu, Y. Meng, R. Lu, S. Zhang and B. Tang, *Chem. Eng. J.*, 2023, **464**, 142650.
17 H. Cao, Y. Li, W. Xu, J. Yang, Z. Liu, L. Bai, W. Yang and M. Yang, *ACS Appl. Mater. Interfaces*, 2022, **14**, 52411–52421.
18 J. Hu, W. Huang, X. Ge, C. Wang, G. Zhang, Y. Chen and C. Tu, *J. Energy Storage*, 2024, **100**, 113485.

19 J. Wu, M. Wang, L. Dong, C. Zhu, J. Shi and H. Morikawa, *ACS Sustain. Chem. Eng.*, 2022, **10**, 7873–7882.
20 A. Ismail, M. Bahmani, X. Chen and J. Wang, *Constr. Build. Mater.*, 2024, **416**, 135289.
21 Y. Zhang, X. Zheng, H. Wang and Q. Du, *J. Mater. Chem. A*, 2014, **2**, 5304–5314.
22 M. Li and S. Liu, *Sol. Energy Mater. Sol. Cells*, 2024, **270**, 112819.
23 L. Chen, J. Lao, J. Ma, Z. He, W. Fu, J. Liu, H. Peng, T. Fang and Y. Luo, *Polymer*, 2025, **319**, 128073.
24 S. Li, W. Ji, L. Zou, L. Li, Y. Li and X. Cheng, *Mater. Today Sustain.*, 2022, **19**, 100197.
25 W. Ji, X. Cheng, H. Chen, L. Li, Y. Li and Z. Liu, *Energy Convers. Manage.*, 2021, **245**, 114637.
26 K. Yuan, J. Liu, X. Fang and Z. Zhang, *J. Mater. Chem. A*, 2018, **6**, 4535–4543.
27 T. K. Maiti, P. Dixit, A. Suhag, S. Bhushan, A. Yadav, N. Talapatra and S. Chattopadhyay, *RSC Sustainability*, 2023, **1**, 665–697.
28 H. Zhang, J. Cai, J. Su, M. Zhu, Y. Gong and B. Xu, *ACS Appl. Nano Mater.*, 2024, **7**, 16360–16371.
29 H. Zheng, P. Li, J. Luo, Z. Wang, J. Wang, S. Ma, W. Guo and J. Wang, *Chem. Eng. J.*, 2025, **520**, 166055.
30 X. F. Wu, Y. Z. Zhang, T. T. Li, H. K. Peng, C. W. Lou and J. H. Lin, *Langmuir*, 2025, **41**, 16736–16747.
31 D. Q. Ng, Y. L. Tseng, Y. F. Shih, H. Y. Lian and Y. H. Yu, *Polymer*, 2017, **133**, 250–262.
32 R. Chen, X. Ge, X. Li, G. Zhang, J. Zhang and X. Ke, *Compos. Sci. Technol.*, 2022, **228**, 109662.
33 X. Yang, C. Liang, T. Ma, Y. Guo, J. Kong, J. Gu, M. Chen and J. Zhu, *Adv. Compos. Hybrid Mater.*, 2018, **1**, 207–230.
34 H. Huang, T. Shi, R. He, J. Wang, P. K. Chu and X. F. Yu, *Adv. Sci.*, 2020, **7**, 2000602.
35 B. Praveen, S. Suresh and V. Pethurajan, *Appl. Therm. Eng.*, 2019, **156**, 237–249.
36 Q. Zhao, F. He, Q. Zhang, J. Fan, R. He, K. Zhang, H. Yan and W. Yang, *Sol. Energy Mater. Sol. Cells*, 2019, **203**, 110204.
37 H. Guo, W. Jiao, H. Jin, Z. Yuan and X. He, *Adv. Funct. Mater.*, 2023, **33**, 1–14.
38 D. Zou, X. Liu, R. He and L. Huang, *Int. J. Heat Mass Transfer*, 2019, **140**, 956–964.
39 N. Mehra, L. Mu, T. Ji, X. Yang, J. Kong, J. Gu and J. Zhu, *Appl. Mater. Today*, 2018, **12**, 92–130.
40 B. Du, M. Wang, Q. Zhao, X. Hu and S. Ding, *Energy Mater.*, 2023, **3**, 300026.
41 S. Matsumura, A. R. Hlil, C. Lepiller, J. Gaudet, D. Guay, Z. Shi, S. Holdcroft and A. S. Hay, *J. Polym. Sci., Part A:Polym. Chem.*, 2008, **46**, 7207–7224.
42 Y. Lin, C. Zhu and G. Fang, *Sol. Energy Mater. Sol. Cells*, 2019, **189**, 197–205.
43 K. J. Thomas, M. Sheeba, V. P. N. Nampoori, C. P. G. Vallabhan and P. Radhakrishnan, *J. Opt. A:Pure Appl. Opt.*, 2008, **10**, 055303.
44 M. M. Gudarzi and F. Sharif, *Soft Matter*, 2011, **7**, 3432–3440.